Chapter 4 Apparent Topographic Height Variations as Measured by Atomic Force Microscopy over a Flat, Differentially Doped Silicon Surface

4.1 Introduction

Atomic force microscopy (AFM) is a technique widely used for measuring surface morphologies [33]. In most high-resolution applications, a non-contact mode is preferred, as it avoids damage or modification to the tip and sample surface caused by physical rubbing or collision. Frequency-modulated non-contact operation relies on the detection of tip-sample interactions that are of longer range than the chemical forces [34,35]. A feedback mechanism is typically employed to keep the cantilever resonance frequency at a fixed offset relative to the free resonance frequency. The resulting topographies are maps of constant force gradient over the sample surface. However, these may, or may not, represent the true surface morphology. Specifically, a surface with different work functions in different regions can give rise to significant variations in electrostatic force that may affect the height measurements [20,36,37,38,39]. This issue has been widely recognized, and a number of models have been proposed to account for the relationship between the apparent heights and experimental parameters [19,40,41,42]. Here, we report a detailed analysis of a particularly simple system, Si(100) surfaces that are topographically flat but with alternately p- and n-doped regions [43]. The different doping give rise to contact potential differences. AFM measurements of these flat surfaces show large apparent topographic height variations up to a few nanometers that depend on the radius, bias polarity, bias voltage, and conducting state of the tip. While the dependence on bias and conducting state is expected because of the electrostatic interaction, the detailed dependence on tip radius is not necessarily obvious. Our observations are well

explained by numerical modeling accounting for all essential interactions and geometrical effects. The results illustrate the interplay of different forces that must be considered for a full understanding of the AFM results.

Atomic force microscopy (AFM) has been routinely used in numerous areas in science and technology. Particularly, true non-contact AFM (NC-AFM) operated in vacuum environment can successfully image delicate structures which can be easily altered by the force exerted in contact AFM, and is frequently employed for application requiring high resolution. In NC-AFM, the forces F_{ts} between the macroscopic nonmagnetic tip and the sample include the chemical forces, the van der Waals force, and the electrostatic force.

The different tip-sample forces enable a variety of operation modes of microscopy and spectroscopy and measures beyond topography [34]. On the other hand, their interplay and dependency on the tip sizes, shapes, and materials of these forces also involve with in complexity in analyses and interpretation of the images. One of known examples is that the topographic height measurements between two regions of different material on a sample by NC-AFM can be off substantially because the tip experiences different residual electrostatic forces on top of the two materials. The electrostatic force originates from the capacitance gradient of the tip-sample system,

$$F_{el} = -\frac{1}{2}\frac{dC}{dz}U^2 = -\frac{1}{2}\frac{dC}{dz}(V_t + V_{cp})^2 , \tag{4.1}$$

where C, U, V_{cp}, and V_t are the representation effective capacitance, effective potential difference (EPD), the local contact potential V_{cp} between the tip and sample, and the bias voltage on the tip, respectively. The contact potential V_{cp} is the difference in work function between the tip and the sample, that is, $V_{cp}=(\Phi_{tip}-\Phi_{sample})/(-e)$ for conducting tips and samples. Often the sample systems subject to the NC-AFM topographic imaging consist of more than

one material with different contact potential. The electrostatic contribution on top of different material is not the same due to the change of V_{cp} over the surface areas of different material and therefore, the topographic height measurement on these sample systems is typically incorrect. However, the quantitative height deviation due to the contact potential difference and the role of the tip's size, shape, and properties in the topographic measurement remain unclear.

Sadewasser *et al.* showed that the correct height measurement on samples with only two different contact potential values is possible by applying an external sample bias of the mean set at the mean contact potential:

$$V_{mcp}=(V_{cp1}+V_{cp2})/2=((\Phi_{tip}-\Phi_{sample1})/(-e)+(\Phi_{tip}-\Phi_{sample2})/(-e)/2=(\Phi_{tip}-(\Phi_{sample1}+\Phi_{sample2})/2)/(-e)$$

[19,20]. In their study, the effect of electrostatic force on the topography measurement is simulated without the van der Waals force and reaches the conclusion that the cone-shaped tip model can well describes their result. Base on the research provided details of the topography height deviation in the frequency-modulated NC-AFM on the samples, consisting of domains of different material for tips of various sizes and external bias. Conclusively, the height deviation depends strongly on the size of the tips when the contact potential cannot be fully compensated. By including the van der Waals force and the electro-static force on the semi-spherical tips in the calculation, we have formulated a systematic way to reasonably estimate the deviation of the height measurement *in situ*.

4.2 Experiment

4.2.1 Sample preparation

In this experiment, scanning tunneling microscopy (STM) and NC-AFM measurements were performed in ultra-high vacuum chamber with a based pressure of 8×10^{-11} torr and equipped with a commercial variable-temperature STM/NC-AFM system. We used commercial heavily doped monolithic Si cantilevers with tip radius of less than 7 nm. The typical force constant k is 42 N/m and free resonance frequency f_0, 260 KHz. Conductive tips have an additional 25-nm thick double layer of Chromium and PtIr5. All images in this work were taken at a cantilever oscillation amplitude (A) of around 16 nm and a frequency shift Δf = -30 Hz.

The samples used are n-type Si(100) wafers with a Phosphorus-doping concentration of 3×10^{14} cm^{-3}. In figure 4.1, a 100-nm-thick thermal oxide [44,45,46] was formed first followed by coating of a 1-μm-thick photoresist. Employing the standard photolithographic technique, the wafers are patterned with areas of micrometer-sized squares and rectangles covered with 50-nm-thick SiO_2 films as a sacrificial layer. Boron (B^+) ion implantation with a dose of 5×10^{14} cm^{-2} was conducted with implant energy of 20-keV except those areas with thick SiO_2 layer. The concentration of Boron impurity introduced near the surface below a 50nm-thick SiO_2 layer is estimated to be about 7.3×10^{18} cm^{-3}. To repair implant damages and substitution incorporation of dopants into the silicon lattice, a 30-min furnace annealing at 850 ℃ after the implantation was performed. The thermal oxide layer was then removed by etching in a HF acid solution, resulting in a hydrogen terminated silicon surface. The surface was cleaned in the mixture of H_2SO_4 and H_2O_2 solutions, and then dipped in 2% HF to remove oxide and simultaneously hydrogen-terminate the surface before inserting into the UHV chamber.

In figure 4.2(a), It shows the mask of the E-Beam written, and can make a pattern form B^+ ion implantation. There is a SEM picture correspond to the mask, and we show the part of

n- and p type as shown in fig. 4.2(b). NC-AFM is used to scan the different area by applying different bias.

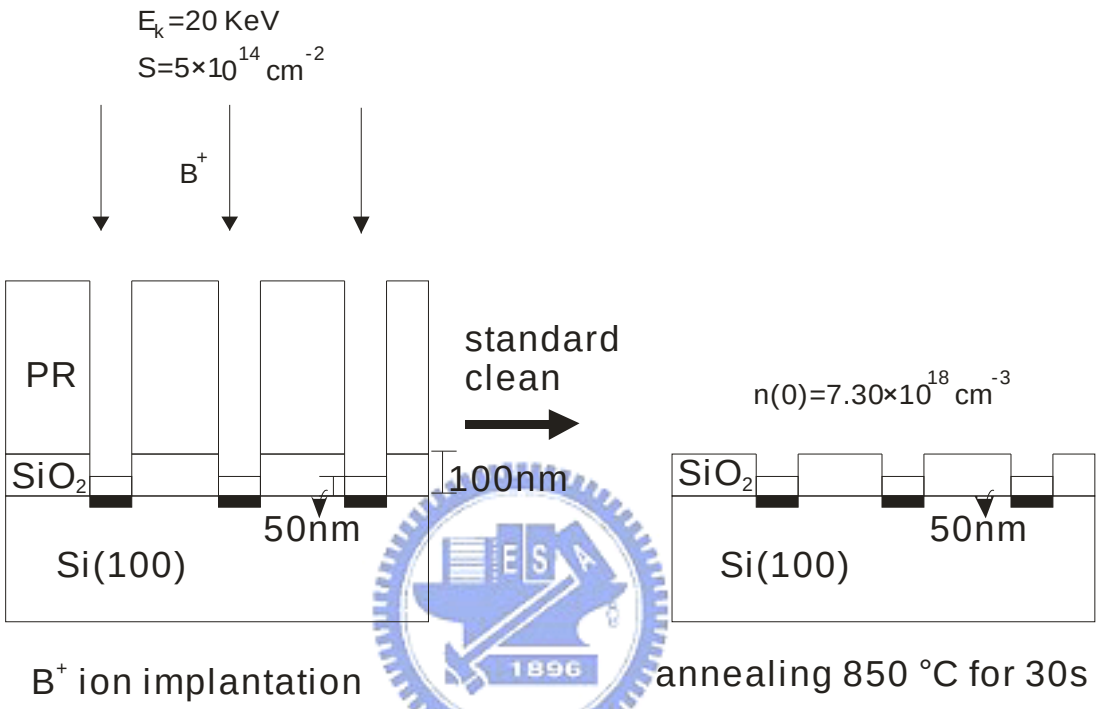

Fig. 4.1 A 100-nm-thick thermal oxide was formed first followed by coating of a 1-μm-thick photoresist. Employing the standard photolithographic technique, the wafers are patterned with areas of micrometer-sized squares and rectangles covered with 50-nm-thick SiO_2 films as a sacrificial layer. Boron (B^+) ion implantation with a dose of 5×10^{14} cm^{-2} was conducted with implant energy of 20-keV except those areas with thick SiO_2 layer. The concentration of Boron impurity appeared near the surface below a 50nm-thick SiO_2 layer is estimated to be about 7.3×10^{18} cm^{-3}. To repair implant damages and substitution incorporation of dopants into the silicon lattice, a 30-min furnace annealing at 850 ℃ after the implantation was performed.

(a)

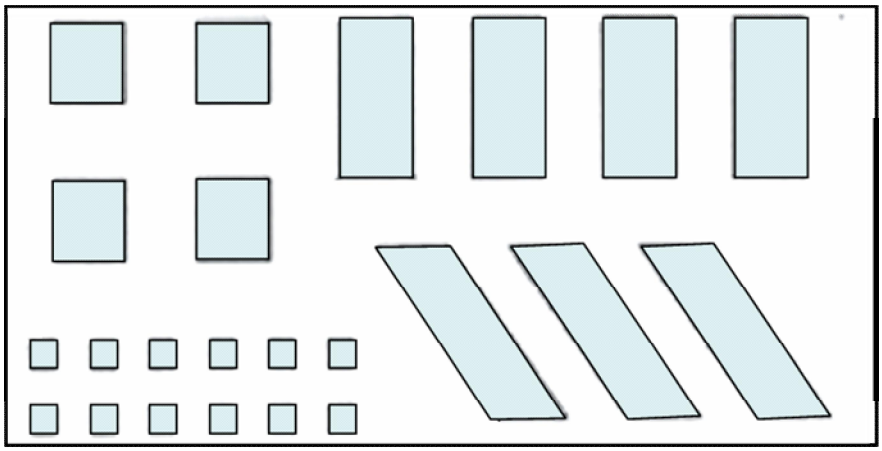

(b)

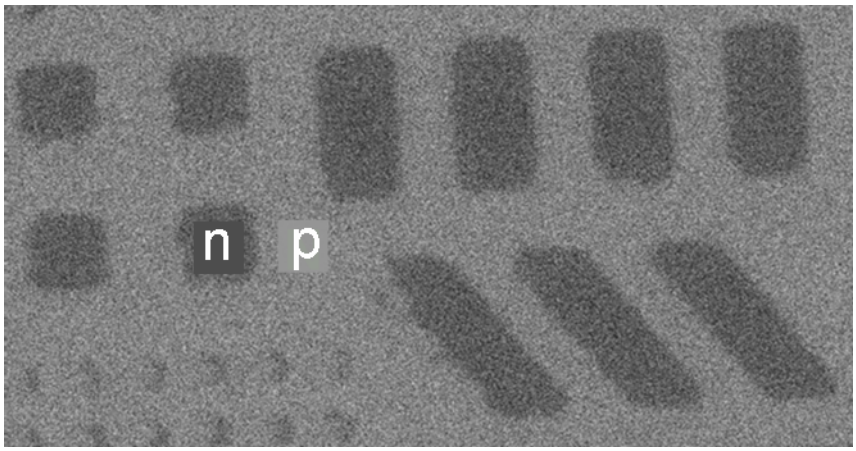

Fig. 4.2 (a) The windows on the mask allow a pattern for ion implantation. (b) SEM micrograph of the Si(100) wafer on the area and corresponding to (a).

4.3 Results and Discussion

4.3.1 The relevant forces and force gradients

The total forces between a nonmagnetic tip and a conducting sample are commonly categorized into the short ranged chemical forces F_{chem}, the van der Waals force F_{vdw}, and the long-ranged electrostatic force F_{el}, i.e. $F_{tot}=F_{chem}+F_{vdw}+F_{el}$. The chemical forces due to the formation of bonding between tip and sample atoms are compatible to other forces only when the tip-sample distance z < 0.5 nm [32,47]. The force-distance calibration curves (d$f(z)$) (not shown here) suggested that the minimum tip-sample distance (D) in this study is in the range of ~1-7 nm; therefore, the chemical force is irrelevant. The electrostatic interaction is difficult to be analyzed due to its strong tip-shape dependence and has been modeled by several groups with different tip geometries.

Scientists such as Colchero, Gil, and Baro has discovered an analytical formula for a realistic tip shape, i.e. a truncated macroscopic conical tip with opening angle q_{tip} with a nanometer- sized paraboloidal tip apex of radius R [48]. In their analysis, $F_{el}=F_{lever}+F_{tr\_cone}+F_{apex}$, where the F_{lever}, F_{tr_cone}, F_{apex} are the electrostatic forces acting on the lever, the cone, and the apex, respectively. Being short range, the van der Waals force between the tip and the sample is found to be dominated by the spherical cap with radius R over an infinite surface: $F_{vdw}=-HR/6z^2$, where H is the Hamaker constant . In all, the total force can be expressed as:

$$F_{tot}(z) = F_{vdw+}F_{apex} + F_{cone} + F_{lever} =$$

$$-\frac{HR}{6z^2}-\frac{pe_0U^2}{1+f(q_{tip})(\frac{z}{R})^2}(\frac{R+\frac{z}{2}}{R-2z})^2(\frac{R-2z}{z[1+2\frac{z}{R}\tan^2(q_{tip}/2)]}+2\ln\frac{4z}{2z+R+(R-2z)\cos(q_{tip})}) \quad (4.2)$$

$$-\frac{4p}{(p-q_{tip})^2}e_0U^2[\ln\frac{z-d/2+h}{z+d/2}-\sin(q_{tip}/2)\frac{z-d}{z-d/2+h}\frac{z-d/2}{z+d/2}]+F_{lever}$$

where $f(q_{tip}) = \frac{\ln[1/\sin(q_{tip}/2)]}{[1-\sin(q_{tip}/2)][3+\sin(q_{tip}/2)]}$; q_{tip} is the cone's full opening angle; h is the macroscopic tip cone of height. The magnitude of these forces and their gradients are calculated and displayed on a logarithm-based scale in Fig. 4.3 and 4.4, respectively. The sketchy straight lines in Figs. 4.3 and 4.4 shows that these force-distance curves approximately follow simple power-law relationship with different exponents. Independent of *U*, the van der Waals force decays with an exponent of -2 as expected. The force on the truncated cone F_{tr_cone}, integrating over the macroscopic shape of the tip, is less sensitive to the tip-sample distance. Because the larger tip apexes lead to the greater truncation of the cone, the force on the tip apex F_{apex} increase with *R* at the expense of F_{tr_cone}. Notably at small distance and large radius *R*, F_{apex} approaches to the force on a simple spherical tip, F_{s_sphere}, with effective radius *R*: $F_{s\_sphere} = \frac{pe_0RU^2}{z^2}$ [49,50,51].

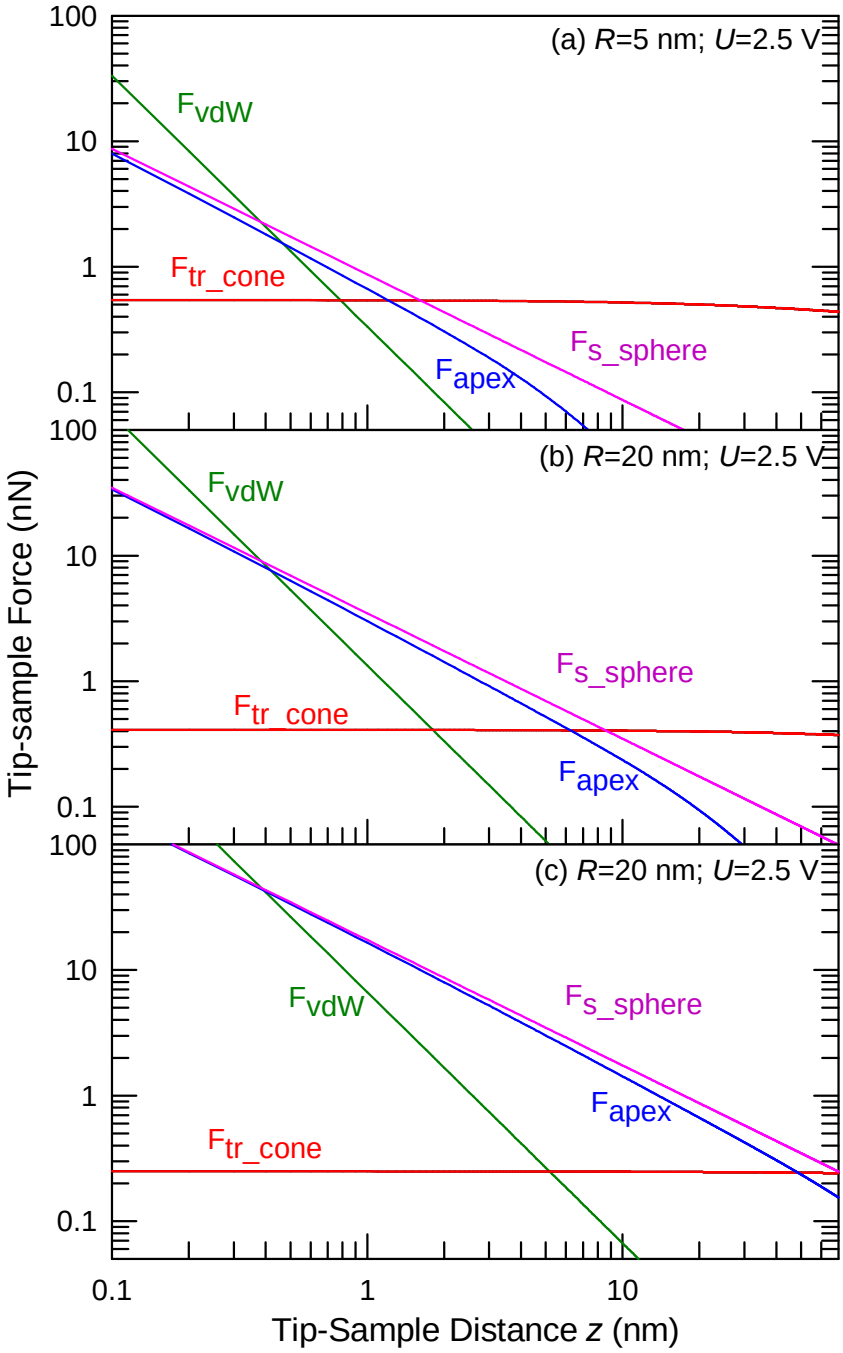

Fig. 4.3 Log-log scale plot of various tip-sample forces for a spherical tip apex with radius (a) 5 (b) 20 (c) 100 nm. The forces have been calculated for $H = 4\times10^{-19}$ J, $U = 2.5$ V, $q_{tip} = 25°$, and $h = 10$ μm.

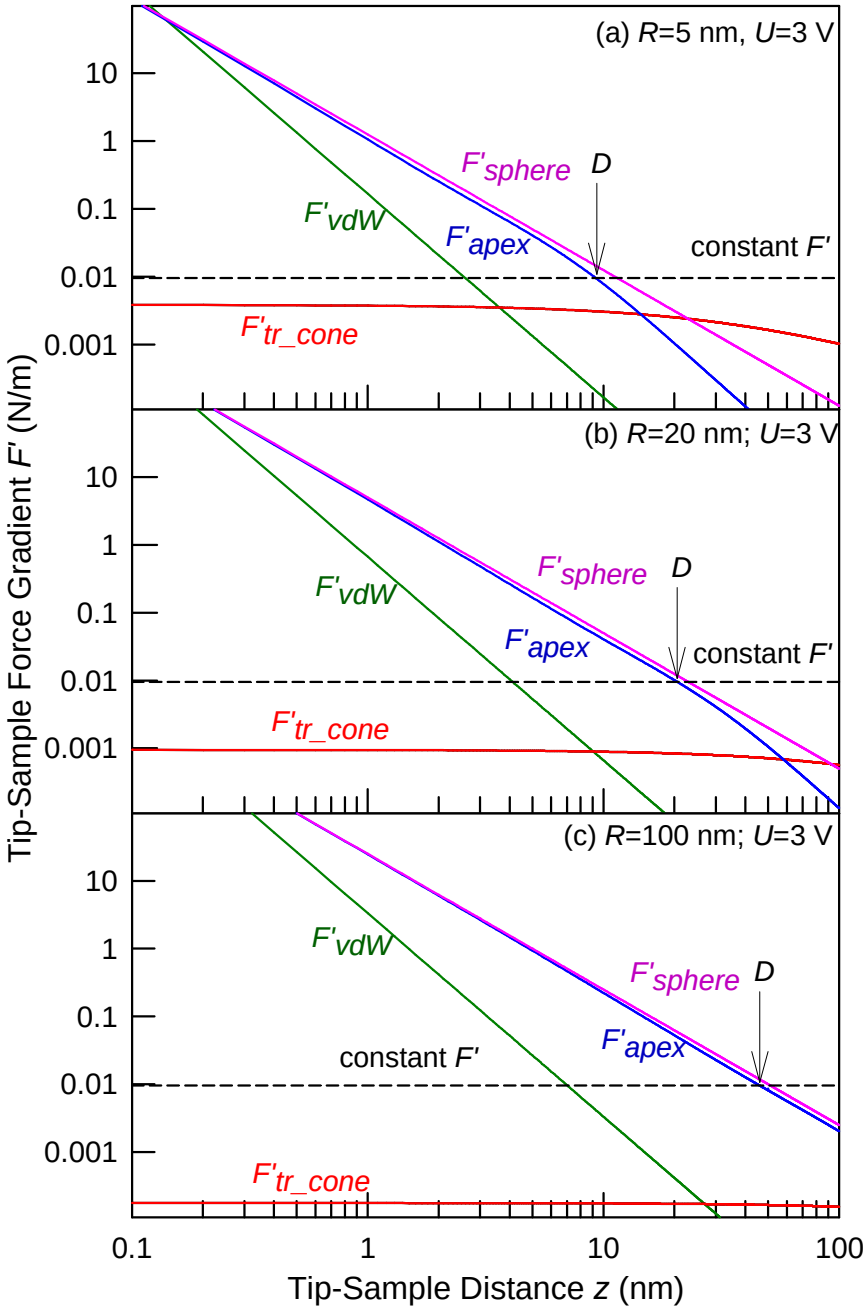

Fig. 4.4 Log-log scale plot of various tip-sample force gradients with tip radius R = (a) 5 (b) 20 (c) 100 nm. The dash line indicates the constant force gradient $F'_{tot} = 9.7\times10^{-3}$ N/m which gives frequency shift of -30 Hz using Eq. (4.3). The arrow points to the minimum tip-sample distance D that satisfies $F'_{vdw} + F'_{apex} + F'_{cone} = 9.7\times10^{-3}$ N/m for a given R and U. Same parameters are used as in Fig. 4.3.

4.3.2 Calculation of the tip-sample distance

In the vacuum environment, the NC-AFM measures the topography of surfaces typically in frequency modulation mode, i.e. the frequency shift Δf with respect of the free resonance frequency f_0 of the cantilever is kept constant by feedback-control of the minimum tip-sample distance $z_{min} = D$ (relative z-height or the apparent topologic height). Assuming that the force gradient $F'_{tot}(z)$ is a constant during the oscillation cycle [52], the frequency shift was proportional to the force gradient $F'_{tot}(z) = F'_{tot}(D)$:

$$\Delta f = -F'_{tot} f_0 / 2k = -(dF_{tot}(D)/dz) f_0 / 2k \tag{4.3}$$

In this case, the image of the constant frequency shift outlined out the contour of constant force gradient F'. Calculated for U = 3 V, f_0 = 260 kHz, Δf = -30 Hz, and k = 42 N/m, the force gradient F'_{tot} is 9.7×10^{-3} N/m and plotted as dash lines in Fig. 4.4. A unique solution $D(R, U=3)$ can be found where $F'_{vdw} + F'_{apex} + F'_{cone} = 9.7\times10^{-3}$ N/m is satisfied. When the magnitude of the effective contact potential increases, F'_{tot} intensifies and the minimum tip-sample distance D would rise in order to keep the frequency shift constant. Accordingly, $D(U, R)$ can be uniquely solved for each U and R; the results is shown in Fig. 4.5(a) for various apex's radius R.

In reality, $F'(z)$ varies rapidly as the tips oscillate with amplitude A~16 nm as Fig. 4.4 illustrates. Utilizing Canonical perturbation theory, the frequency shift as a function of D was related to the weighted average force over an oscillation cycle [53,54]:

$$\Delta f(D) = -\frac{f_0^2}{kA^2}\int_0^{1/f_0} F_{tot}[D + A + q'(t)]q'(t)dt \tag{4.4}$$

where $q'(t)=A\cos(2p\,f_0\,t)$ is the cantilever deflection.

With known f_0 = 260 kHz, Δf = -30 Hz, and k = 42 N/m, a unique solution D for each U and R can be again found from Eq. (4.3); the result was plotted in Fig. 4.5(b). The obvious difference between Figs. 4.5(a) and 4.5(b) is that the tip sample distances at U = 0, that is, $D(0)$ in Fig. 4.5(a) are larger than those in Fig. 4.5(b) for the same $H = 4\times10^{-19}$ J. The force-distance calibration curves ($df(z)$) suggests that $D(0)$ are close to the value found in Fig. 4.5(b). The over estimation of $D(0)$ in using Eq. (4.3) is evident since it uses the largest force gradient (F'_{vdw}) in an oscillation cycle for the calculation. Using a smaller H effectively reduces the overestimation of the F_{vdw} as shown by the red lines in Fig. 4.5(a). Compared with those in Fig. 4.5(a), the $D(U)$ curves for small R_s have smaller curvatures in Fig. 4.5(b). This can be attributed to the cancellation of the increasing electrostatic force by the van der Waals force at smaller D found in Fig. 4.5(b).

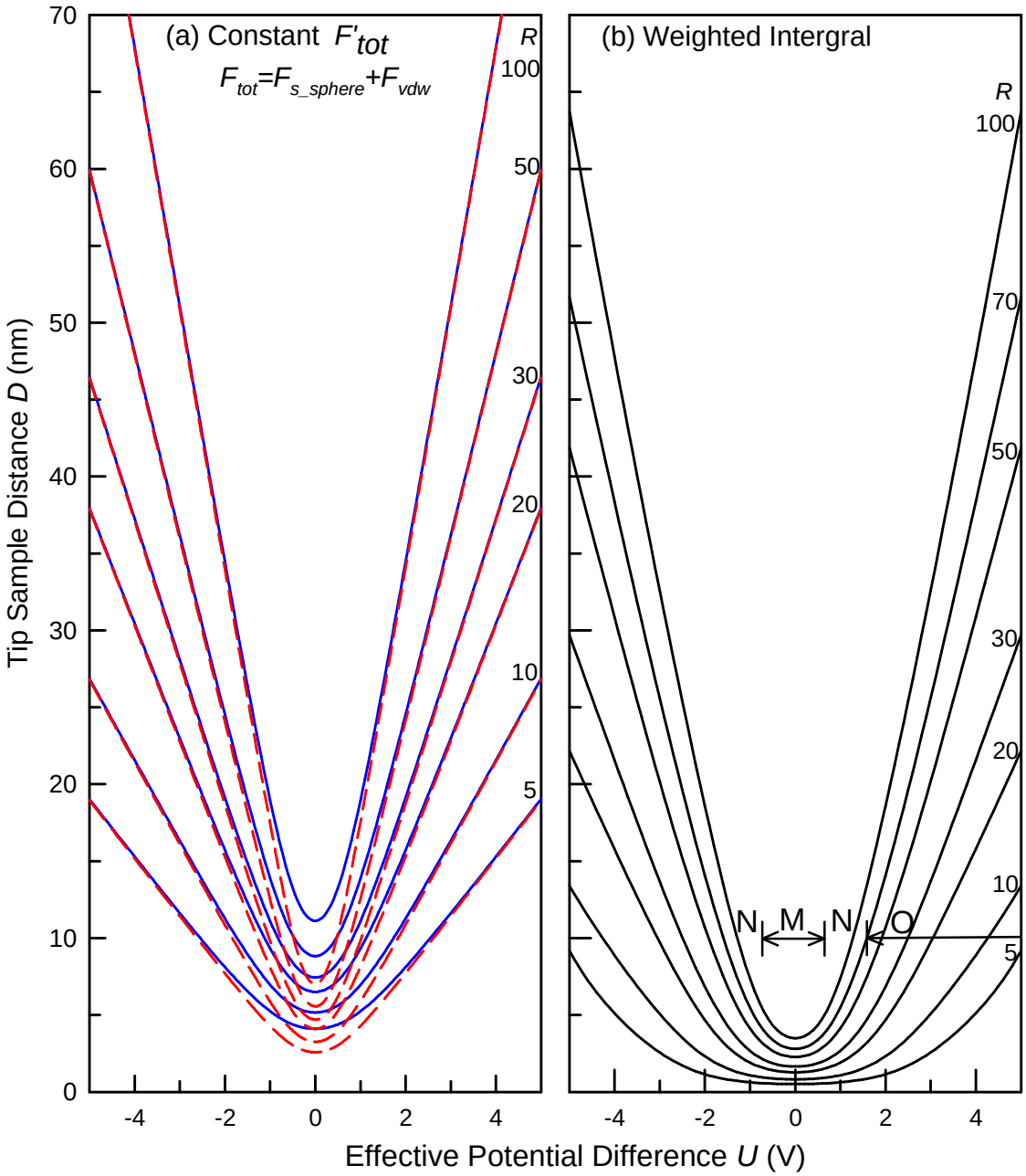

Fig 4.5 The minimum tip-sample distance D solved from (a) Eq. (4.3) and (b) Eq. (4.4) for f_0 = 260 kHz, Δf = -30 Hz, k = 42 N/m, and various tip radius R as indicated. M, N, and O denote regions with $|U|$ in the interval [0, 0.7], [0.7, 1.6], and [1.6, 5.4], respectively. The blue and red lines in (a) were obtained with $H = 4\times10^{-19}$ (solid-line) and 1×10^{-19} (dash-line), respectively.

In Eq. (4.4), the weighted integral of the total force over an oscillation cycle indicates that each component force can contribute to the constant frequency shift Δf. Given a spherical tip apex with radius R and effective contact potential U and the minimum tip-sample distance $D(R,U)$ over an oscillation cycle in Fig. 4.6(b), the relative contributions of each component forces can be separately derived. Examples of these contributions verse EPD are plotted in Figs. 4.6(a) and 4.6(b) for a typical tip radius R = 20 nm and a sharp tip radius R = 5 nm, respectively. For convenience of this discussion, Figs. 4.6(a) is divided into four characteristic regions of M, N, O, and P. In Region M, $|U|$ <0.7 V and the van der Waals term predominates (>75%). In Region O where 1.6 V< $|U|$ <5.4 V, the electrostatic contribution to Δf from the tip apex outweighs while the electrostatic contribution from the truncated cone becomes increasingly significant. Region N is the transition region between M and O in which the dominating contribution from the van der Waals force crosses over to the electrostatic force. As a comparison, the van der Waals term for small tip radius of 5 nm in Fig. 4.6(b) contributes more than 75% for $|U|$ up to 1.0 V and the electrostatic force from the tip does not contribute predominantly as that from the truncated cone abruptly increases as $|U|$.

In Fig. 4.6, D is minimal at U = 0 because of zero electrostatic force for all R. When electrostatic forces increase with the magnitude of the effective contact potential, the tip-sample distance D would enlarge in order to keep the frequency shift constant. $D(U)$ in region M is slow-varying because the increase in the electrostatic contribution to Δf is largely compensated by the reduction of the van der Waals force. In region O, the tip-sample force gradient for $R \geq$ ~20 nm is mainly contributed by the apex:

$$F'_{tot} \approx F'_{apex} \approx F'_{s\_sphere} = p e_0 R \left(\frac{U}{z} \right)^2 \tag{4.5}$$

as shown in Fig. 4.3. Since the total force depends on the quotient of U and z, the tip-sample

distance appears as a straight line in Region O, that is, as Fig. 4.6 displays.

$$\Delta z = \sqrt{\frac{pe_0 Rf}{2k|\Delta f|}}\Delta U \tag{4.6}$$

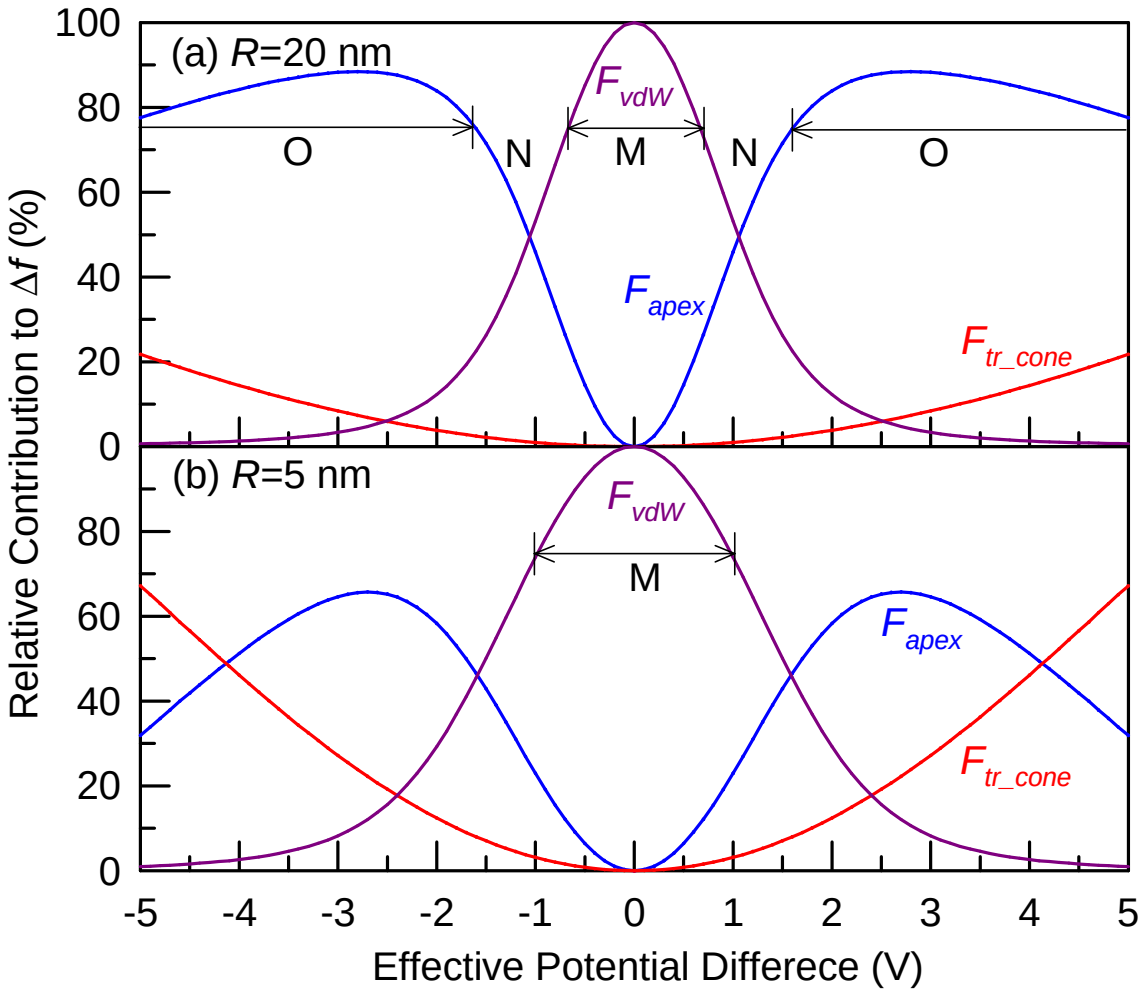

Fig. 4.6 Individual contribution to Δf from various component forces as indicated. Parameters: $H = 4\times10^{-19}$ J, $q_{tip} = 25°$. In (a), the regions labeled M, N, and O are defined as in Fig. 4.5. M and O defines a region where F_{vdw} and F_{apex} contribute more than 80% to Δf, respectively. N denotes the transition region between M and O.

4.3.3 The origin of incorrect *z*-height measurement

To illustrate the origin of incorrect *z*-height measurement in NC-AFM, consider that a tip with an apex of radius R = 20 nm and a bias V_t scans over an atomically flat conducting surface as shown in Fig. 4.7(a). The sample surface has two kinds of domains that consist of similar materials M_1 and M_2 whose work function is Φ_{s1} and Φ_{s2}, respectively. With the same tip, the tip-sample distance is the same on the two domains at a given U: $D_1(U) = D_2(U)$. Assuming that the contact potential difference between the tip and M_1 and M_2 is V_{cp1} = -0.1 V and V_{cp2} = 0.1 V. With a given V_t, the tip-sample distance curves on the two domains, that is, $D_1(V_t)$ and $D_2(V_t)$, would be the same aside from a horizontal offset of $\Delta U = U_2 - U_1 = \Phi_{s2} - \Phi_{s1} = \Delta\Phi$ =0.2 eV as shown in Fig. 4.7(b). Upon scanning laterally with bias V_t, a tip experiences a change in EPD, that is, ΔU at the domain boundary of M_1 and M_2. Under the same feedback condition, the tip would response to the change in EPD by varying the tip-sample distance by an amount $\Delta D(V_t) = D_2(V_t) - D_1(V_t)$, leading to a step-like response at the domain boundary. In other words, the topographic height profile would have an apparent *z*-height difference $\Delta z(V_t) = \Delta D(V_t)$ between the two domains even though the surface is actually flat.

In Fig. 4.7(b), the apparent topographic height deviation Δz is insignificant in Region M since the dominating van der Waals force of this region is in the independent of U and the electrostatic forces are small. In region N, ΔD rises with the electrostatic forces and approaches a constant in region O where the D_1 and D_2 curves are nearly parallel with a constant slope as shown in Eq. (4.4). The apparent topographic height deviation ΔD varies not only with V_t but also with R and ΔU, as calculated and shown in Fig. 4.8. As Figs. 4.8(a) and 4.8(b) illustrate, $\Delta z(V_t)$ is an odd function of V_t with respect to V_{mcp} (0 in this case). For tips with small radius, the U-independent van der Waals force is the main source of the frequency shift and the tip's *z*-height changes little at the M_1-M_2 domain boundary. For tips with R > ~20

nm, $\Delta z(V_t)$ rapidly increases with $|U|$ initially, but reaches a plateau at $|U|$ > ~2 V, again due to the dominant role of the electrostatic force from the tip. As Fig. 4.8 illustrates, the height of the plateau, Δz_m (We choose $\Delta z_m = \Delta z$ (V_t = 2.5 V) since this is the region that F_{apex} dominates.) increases with R and Δf ; the value of Dz_m was calculated and plotted in Fig. 4.9 for both the simplified constant $F_{ts}^{'} = (F_{s\_sphere} + F_{vdW})'$ model and the comprehensive weighted integral model. The two models give similar trend except that the simplified constant model gives a noticeably larger Δz_m in the case that the two domains have large work function difference.

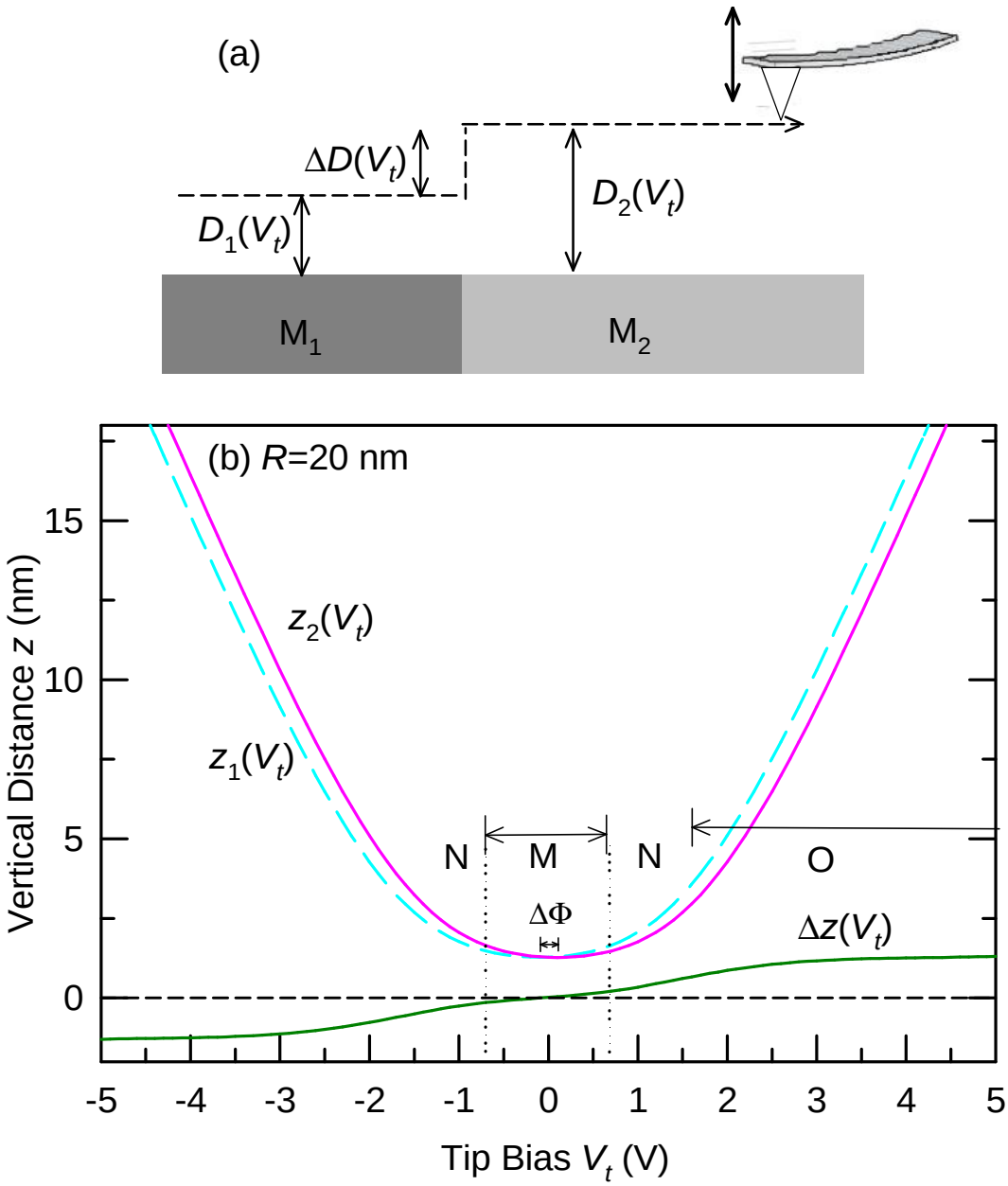

Fig. 4.7 (a) Schematic diagram showing a line profile when a tip scans over a flat conducting surface. The sample surface has two kinds of domains that consist of similar materials M_1 and M_2 with different work functions. V_t is the bias voltage applied on the tip. Experiencing different electrostatic forces, the tip move forwards/backwards at the domain boundary in the constant frequency shift mode. (b) Tip-sample distances as a function of V_t on M_1 (cyan-long dash-line) and M_2 (pink-solid-line) and their differences (underneath green-line).

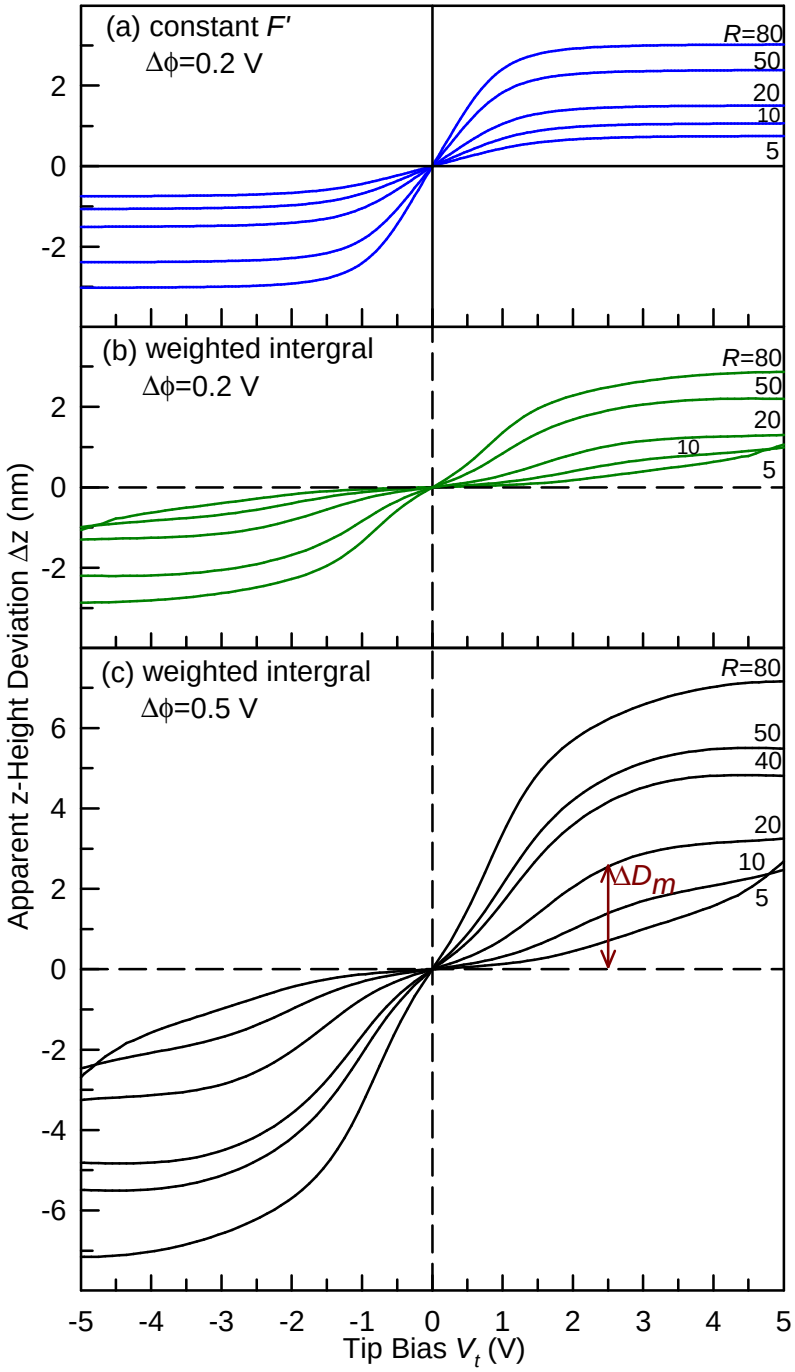

Fig. 4.8 The apparent topographic height deviation Δz as a function of V_t for various R. The scanning condition is demonstrated in Fig. 4.7(a). M_1 and M_2 is assumed to have a zero mean V_{cp} (V_{mcp} = 0 V) with the tip and a work function difference Δf of (a) 0.2 V and (b) 0.2 V. In (c) the double arrow labeled Δz_m indicated the choice as the plateau height.

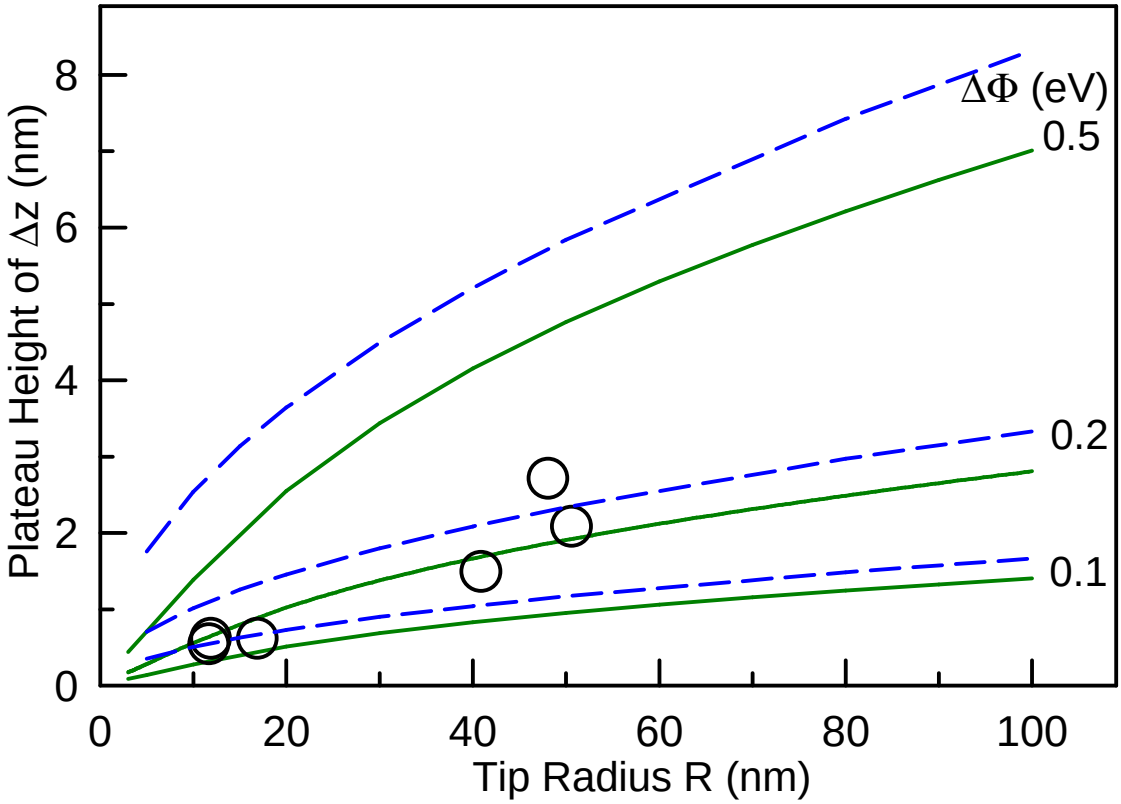

Fig. 4.9 The height of the plateau in Δz, $\Delta z_m(V_t = 3\ V)$ measured (open circles) and calculated for the comprehensive weighted integral model (magenta-solid-line) and the simplified constant-force-gradient model (blue-dash-line) for various work function Δf as indicated.

4.3.4 Experiment observation

Figure 4.10 demonstrates four set of STM and NC-AFM images on the patterned hydrogen-passivated silicon surface; each set was obtained by the same cantilever (labeled Tip I-IV) without much change in the tip shape during the scan with care. A square n-type area of ~3×3 μm^2 is located near the center of each image and surrounded by p-type silicon. STM images (Fig. 4.10(I_a, II_a, IV_a) show that the entire scanned area was essentially flat. The *z*-height profiles $z(V_t)$ (or relative tip-sample distance curves $D(V_t)$) on both areas were also measured as a function of tip bias while maintaining a constant Δf as shown in Fig. 4.11.

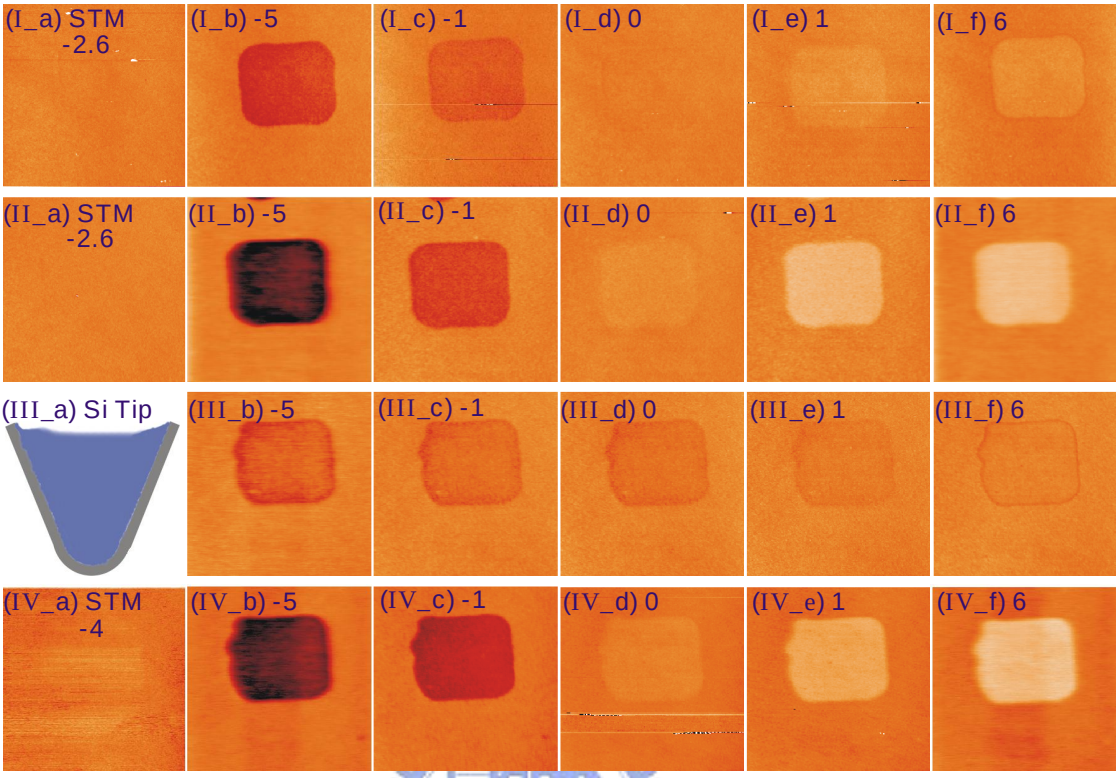

Fig. 4.10 STM (labeled) and NC-AFM images for a diluted HF-etched Si(100) substrate with tip bias as indicated in volt. The 3×3 μm^2 area near the center of each image is n-type and surrounded by B^+-implanted p-type areas. The images are of size 6×6 μm^2 and have a color scale for z ranging from -4 to 3 nm. The frequency shift is -30 Hz. Set I and II were taken with PtIr5-coated tips of different radii. Set III and IV were taken with the same heavily doped Si tip, showing schematically in (III_a) with a SiO_2 layer (grey) of a few nanometers. Before imaging Set IV, the Si (blue) tip was pushed onto the sample and scratched off the oxidized layer on the tip intentionally.

4.3.5 The tip-sample distance curves using conduction tips

In Figs. 4.11(a) and 4.11(b), the line shapes of the two curves on the n- and p-type areas are largely the same due to the same tip-sample interactions. When the electrostatic force F_{el} vanishes at $V_t = -V_{cp}$, a tip experiences only the F_{vdW} and the tip's z-height reaches its minimum. For the conducting PtIr5 tips, the measured V_{cp} difference between n- and p-silicon was about 0.2 V, close to the value found with Kelvin force microscopy (KFM) [unpublished]. The value of V_{cp} is smaller in that the contact potential of about 0.7 V ($V_0 = 0.0259\times\ln(N_aN_d/2.25\times10^{20}$ V) is expected for a bulk silicon pn junction; it is likely reduced by the surface/defect states on the HF-etched surface [55].

The measured tip-sample distance curves on both the n- and p-type areas, z_n and z_p in Figs. 4.11(a) and 4.11(b), increase relatively linear in Region O, as Eq. (4.6) in Sec. 4.3.2 suggests. However, the curves exhibit a small asymmetry on two sides of EPD. Because both z_n and z_p reveal the same trend, this asymmetry could be related to the contribution of the surface state capacitance into the effective capacitance in Eq. (4.1) [56].

From the slope of these curves, the radius R of the tip apex and the corresponding tip-sample distance curves can be readily calculated, as also shown in Fig. 4.11. Notably, the spherical tip model gives a smaller tip radius for the same slope. However, the curves calculated from this simplified model show no curve-up feature at large U, a characteristics that is predicted by including the truncated-cone contribution but is not observed experimentally. Despite of the reasonable overall agreement of the line shapes, the measured line shapes for small $|U|$ (Region M in Fig. 4.5) in Fig. 4.11(a) and 4.11(b) have curvatures in between those calculated from the weighted integral model and the simplified spherical model. Such finding has anticipated since the forces at small tip-sample distances depends strongly on the exact tip-shapes and the approximation used in our formula generally does not

apply well.

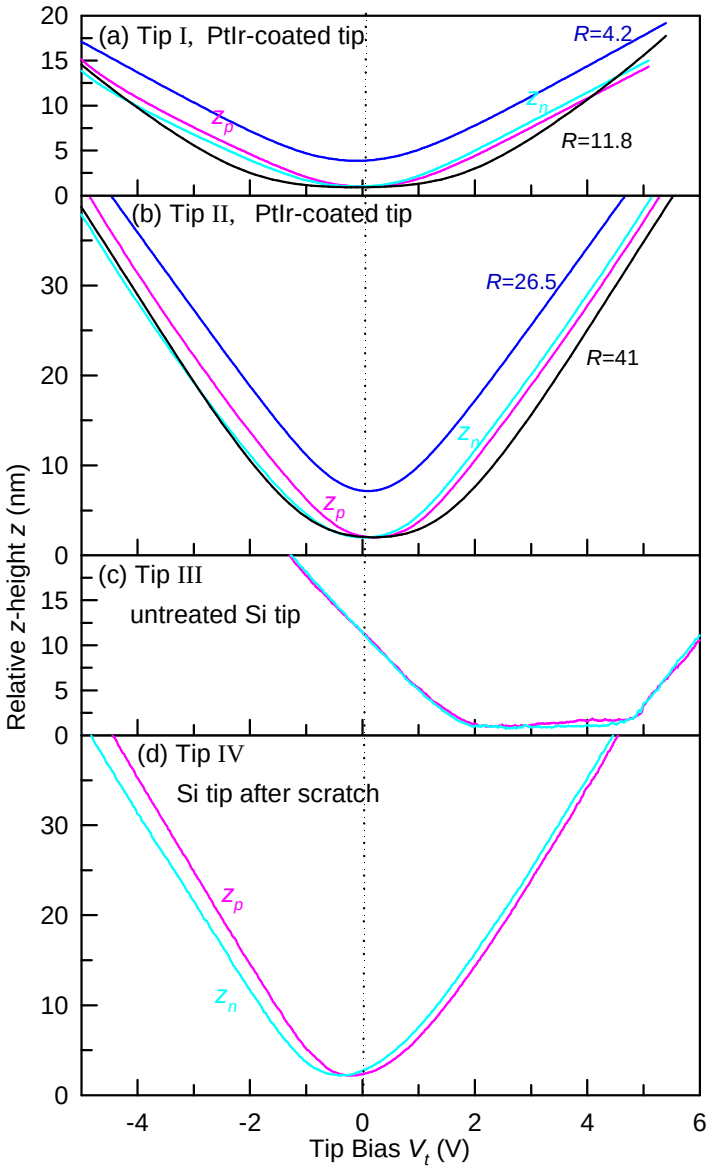

Fig. 4.11 Relative *z*-height (tip-sample distance *D*) versus tip bias measured on the n-type (z_n, cyan) and p-type (z_p, pink) domains for the same tips used in the four set of images in Fig. 4.10. The blue and black curves are results from Eqs. (4.3) and (4.4) calculated with *R* that gives the same slope with experimental curves at the vicinity V_t = 3 V. The large offset in the V_{cp} in (c) is due to external charge on the oxide layer of the Si tip (Fig. 4.10 III_c). The dash line in (c) is the result of fitting assumption that an oxide thickness of 7 nm covered the conducting tip apex.

4.3.6 The apparent *z*-height deviation using conduction tips

Although STM images in Fig. 4.10 indicate that the scanned areas were flat; however, the n-silicon squares in the NC-AFM images appear either lower (darker) or higher (brighter) than p-silicon surrounding depending on the tip bias. The difference of the apparent z-height between the n- and p-type area, that is, $\Delta z(V_t) = z_n - z_p$, can be obtained directly from images and indirectly by subtracting z_n from z_p results in the apparent z-height difference of tips on the n- and p-type regions. As shown in Fig. 4.12(a) and 4.12(b), $\Delta z(V_t)$ is null at V_{mcp}, increases initially, and then reach a plateau as V_t moves away from V_{mcp}. The apparent topographic height deviation between the two regions can be calculated with the tip radius obtained from fitting the tip-sample distance curves in Fig. 4.11 as discussed in Sec. 4.3.3. The results, also shown in Fig. 4.12, are matched with those obtained experimentally on the positive side of U. The additional capacitance effect of surface states likely is responsible for destroying the symmetry of electrostatic potential difference on the negative side.

4.3.7 Using nonconductive tips

As discussed in the previous sections, the apparent height deviation results from the capacitive force between conducting tips and samples. Using dielectric tips is a seemingly simple way to remove the error in the *z*-height measurement. In fact, a thin oxide layer is typically formed on commercial Si tips in air. The native oxide of thickness d_{ox} provides the van der Waals interaction F_{vdW} at a shorter tip-sample distance than the conducting heavily doped Si materials inside by d_{ox} as illustrated in Fig. 4.10(III_a). If d_{ox} is large enough, the dominating F_{vdW} would result in V_t-independent *z*-height curves at small voltage for both M_1 and M_2 regions and therefore, no z-height deviation would occur. In deed flat $\Delta z(V_t)$ was observed (unpublished). However, external charges on the dielectric layer can often be

trapped near the tip apex or the Si-oxide interface, leading to an additional offset in effective potential, i.e., $U = V_t+V_{cp}+V_{offset}$. As shown in Fig. 4.11(c), both the z_n and z_p curves, having their symmetry center at $V_{cp}+V_{offset}$ = ~ -3.2 V, are rather flat within a range of 1.5 V and increases with $|U|$ beyond that range. A fairly good fitting to Eqs. (4.2) and (4.4) is shown in Fig. 4.11(c) with R = 7 nm and d_{ox} = 7 nm.

In the Fig. 4.11(c), the results taken with tip III illustrate much smaller height variations. Separated by the nonconducting native oxide layer in addition to D, the distance between the conducting parts of the tip and the sample is larger than that of a conducting tip with the same tip geometry. The electrostatic interaction is therefore, significantly reduced while the van der Waals contribution remains near constant. The dashed curve shown in Fig. 4.12(c) is obtained by assuming a 7-nm-thick oxide on a conducting body with an apex radius of 7 nm based on the manufacturer's specifications. Within _ ±3 V, the tip-sample distance remains fairly constant because F_{apex} and F_{cone} are insignificant at such small biases and the van der Waals term is insensitive to potential changes. This model leads to the calculated curve shown in Fig. 4.11(c), which well supported with the data.

The existence of native oxide on Si tip and its role in NC-AFM can be further verified with its removal. To scan the surface with a large speed, for example, can effectively remove the native oxide in situ and turn the scanning tip apex into conducting doped silicon. As shown in Figs. 4.11(d) and 4.12(d), V_{offset} is basically removed and the z_n, z_p and Δz curves exhibit similar behavior as those for PtIr5 tips.

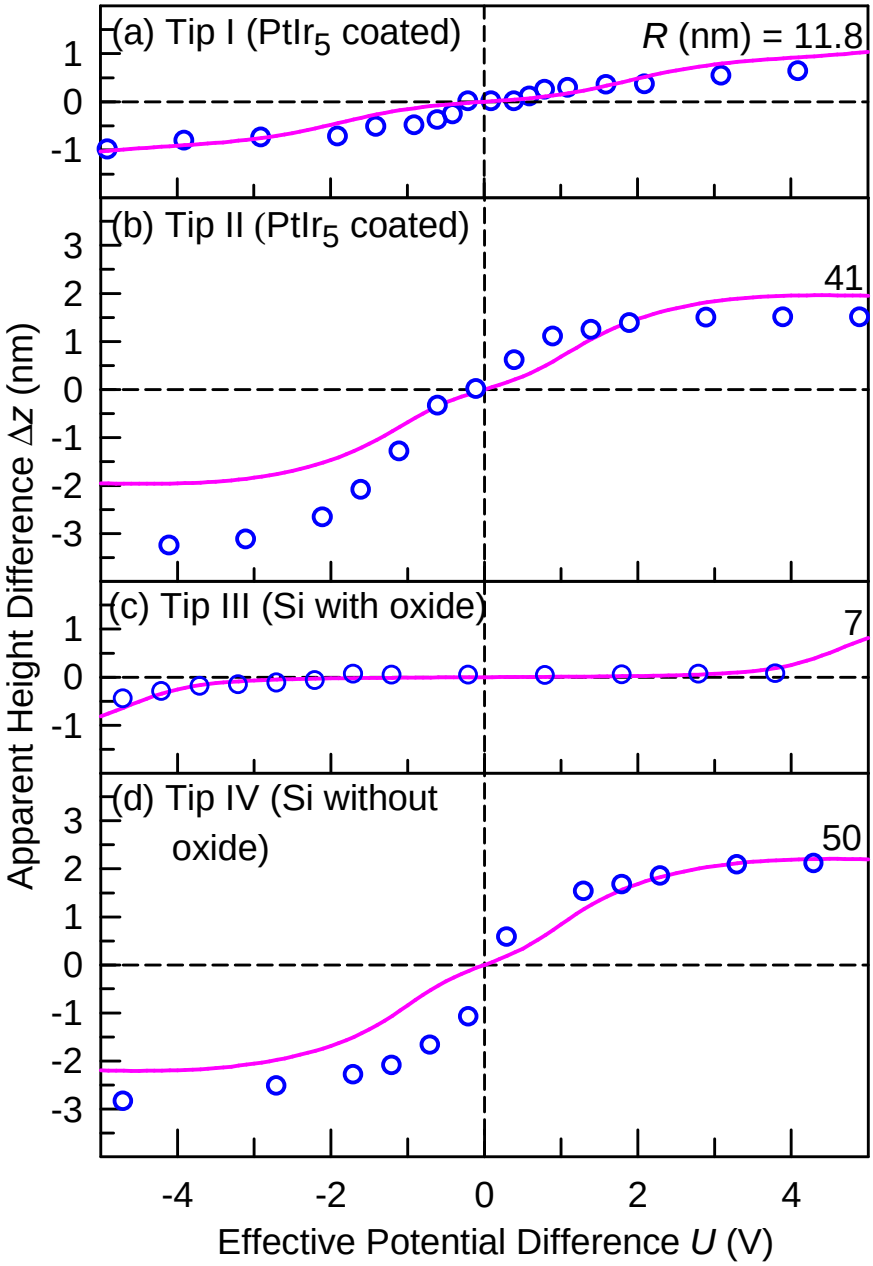

Fig. 4.12 Apparent z-height differences $\Delta z = z_n - z_p$ (open circles and black curves) obtained from the NC-AFM images in Fig. 4.10 between the n-p domains and results of subtraction from the z_n and z_p curves in Fig. 4.11. The two domains have the same height in the STM images.

4.4 Conclusion

In conclusion, we have performed a detailed study of the response of an AFM operating in a frequency-modulated non-contact mode that is widely employed in surface morphology measurements. The objective is to achieve a level of quantitative understanding of the effects and interplay of the various contributions to the force between the tip and sample. With a test sample of Si(100) that is topographically flat but with a surface pattern of alternately doped areas, we have experimentally examined the effects of the work function variations on the apparent topographical height as a function of the radius, bias, and conducting state of the tip. The results show large apparent topographical variations with seemingly complex functional relationships. The results are nevertheless well explained by a full analysis accounting for all essential interactions in the system.